SCIENCE CHINA
Physics, Mechanics & Astronomy

•Article•

June 2019 Vol. 62 No. 6: 967812
https://doi.org/10.1007/s11433-018-9329-4

Turning $ZrTe_5$ into a semiconductor through atom intercalation

QiYuan Li[1], YangYang Lv[2], JingHui Wang[1], Song Bao[1], Wei Shi[1], Li Zhu[1], WeiMin Zhao[1], ChengLong Xue[1], ZhenYu Jia[1], LiBo Gao[1,3], YanBin Chen[1,3], JinSheng Wen[1,3], YanFeng Chen[2,3], and ShaoChun Li[1,3*]

[1]*National Laboratory of Solid State Microstructures, School of Physics, Nanjing University, Nanjing 210093, China;*
[2]*National Laboratory of Solid State Microstructures, Department of Materials Science and Engineering, Nanjing University, Nanjing 210093, China;*
[3]*Collaborative Innovation Center of Advanced Microstructures, Nanjing University, Nanjing 210093, China*

Received October 12, 2018; accepted November 19, 2018; published online February 25, 2019

In this study we successfully intercalated potassium (K) atoms into single $ZrTe_5$ crystals by liquid ammonia method, and found a semimetal-to-semiconductor transition at low temperatures in K-intercalated $ZrTe_5$. As the K concentration increased, the resistance anomalous peak was gradually suppressed until finally disappearing. Whilst, the corresponding Hall resistance measurements consistently showed a sign reversal. The semimetal-to-semiconductor transition can be attributed to a lattice expansion induced by atom intercalation, leading to a larger energy band gap.

$ZrTe_5$, atom intercalation, topological insulator, magnetoresistance, Hall resistance

PACS number(s): 71.30.+h, 72.20.-I, 75.47.-m

Citation: Q. Y. Li, Y. Y. Lv, J. H. Wang, S. Bao, W. Shi, L. Zhu, W. M. Zhao, C. L. Xue, Z. Y. Jia, L. B. Gao, Y. B. Chen, J. S. Wen, Y. F. Chen, and S. C. Li, Turning $ZrTe_5$ into a semiconductor through atom intercalation, Sci. China-Phys. Mech. Astron. **62**, 967812 (2019), https://doi.org/10.1007/s11433-018-9329-4

1 Introduction

Zirconium pentatelluride ($ZrTe_5$) elicited the interest of the scientific community about three decades ago due to its potential applications in thermoelectricity, resistance anomaly, etc. [1-8]. Recently, $ZrTe_5$ has attracted increasing attention because of its mysterious topological nature. Density Functional Theory (DFT) calculations predicted that single-layer $ZrTe_5$ is an ideal two-dimensional topological insulator (TI) with an indirect band gap of ~0.1 eV [9]. Conversely, the topological characteristics of its bulk counterpart resides near the boundary of a topological phase transition from weak to strong TI passing through a 3D Dirac semimetal state [9-11]. Even though great efforts have been devoted to experimentally verify the topological characteristics of bulk $ZrTe_5$, these are still under debate: weak TI, strong TI, or Dirac semimetal have all been proposed as states based on experimental observations with different techniques [12-32]. Thus, a bulk band gap and a topological edge state were detected by ARPES and by STM [14,15,29], suggesting that $ZrTe_5$ is a weak TI. Controversially, signatures of 3D Dirac semimetal were demonstrated by magnetoresistance (MR) [18-20,32] and magneto-infrared spectroscopy measurements [12,13,17,24,25]. A strong TI state was also proposed for bulk $ZrTe_5$ [21,27]. In addition, more unusual physical properties have been observed in bulk $ZrTe_5$, such as the Zeeman splitting [20,33,34], the chiral magnetic effect (CME) [16], the 3D quantum Hall effect (QHE) [35], the

*Corresponding author (email: scli@nju.edu.cn)

© Science China Press and Springer-Verlag GmbH Germany, part of Springer Nature 2019

anomalous Hall effect (AHE) [36], the giant planar Hall effect (GPHE) [37], and the discrete scale invariance (DSI) [38,39].

Considering the extreme sensitivity of the $ZrTe_5$ band structure on the lattice constant, the above mentioned experimental divergence may be due to difference in sample growth. It is worth noting that the Dirac node of $ZrTe_5$ is not protected by crystal symmetry, and a band gap can be opened by a perturbation turning it into a topological insulator. High pressure was applied to tune $ZrTe_5$ into a superconductor [40], and to induce a topological phase transition [41]. The exfoliated $ZrTe_5$ nanosheet exhibits metallic behavior and a tunable resistance maximum, which can be ascribed to the dependency of the band structure on thickness [42,43]. Up to now, most of the studied $ZrTe_5$ bulk samples, grown by chemical vapor transport (CVT), behave as a metal at low temperatures, and the resistance maximum is located at ~130-150 K, which indicates that the bulk states of $ZrTe_5$ contribute to its electrical conductivity. A recent study showed that such metallic state may be induced by intrinsic Te defects induced during CVT growth, and the flux growth method may help to reduce such defects, thus realizing semiconductors at low temperatures [44].

In this study, we successfully intercalated potassium (K) atoms into $ZrTe_5$ single crystals by the liquid ammonia method, which allows to gradually tune the electronic structure of $ZrTe_5$. Electrical transport measurements showed a smooth transition from metallic to semiconducting behavior at low temperatures upon increasing the potassium concentration, which is accompanied by the suppression of the resistance peak. Raman spectroscopy measurements indicated that the van der Waals gap in $ZrTe_5$ is enlarged by the intercalation of K atoms, which is akin to negative (tensile) pressure applied along the *b*-axis. Therefore, it can be concluded that such metal-to-semiconductor transition is induced by the enlarged band gap that results from lattice expansion. Furthermore, the Hall resistance measurements consistently showed a sign reversal between 120 and 160 K irrespective of whether the resistance peak was suppressed or not, suggesting that carrier type reversal can occur even in the absence of an anomalous resistance peak.

2 Experimental methods

Single $ZrTe_5$ crystal was grown by CVT method with iodine (I_2) as the transport agent, as described in a previous study [45]. The K-intercalated $ZrTe_5$ sample was obtained by the liquid ammonia method [46,47]. Firstly, the single $ZrTe_5$ crystal and the potassium sheet were placed into a quartz tube. Secondly, the quartz tube was sealed and vacuumed, and then placed into a cold trap containing an alcohol/water mixture. Subsequently, high-purity ammonia gas (99.999%) was introduced into the quartz tube and condensed as liquid ammonia, immersing the samples. The potassium sheets were dissolved in liquid ammonia, and the atoms were intercalated into the $ZrTe_5$ single crystal. After the intercalation, the liquid ammonia was pumped away. Electrical resistance measurements were conducted in a physical property measurement system from Quantum Design. Raman spectra were recorded on a WITec Alpha 300R with a 532-nm laser.

3 Results and discussion

The crystal structure of the single $ZrTe_5$ crystal having K atoms intercalated within the van der Waals gap is illustrated in the inset of Figure 1. $ZrTe_5$ is a quasi-two-dimensional layered material with an orthorhombic crystal structure belonging to the *C*mcm (D_{2h}^{17}) space group [1,48]. In a single-layer $ZrTe_5$ sheet each Zr atom is surrounded by three Te atoms forming a $ZrTe_3$ triangular prism along the *a*-axis. These $ZrTe_3$ triangular prisms are linked by parallel zig-zag Te chains along the *c*-axis, thus forming a quasi-two-dimensional *a*-*c* plane. Bulk $ZrTe_5$ consists of these sheets stacked along the *b*-axis and held together by van der Waals interactions.

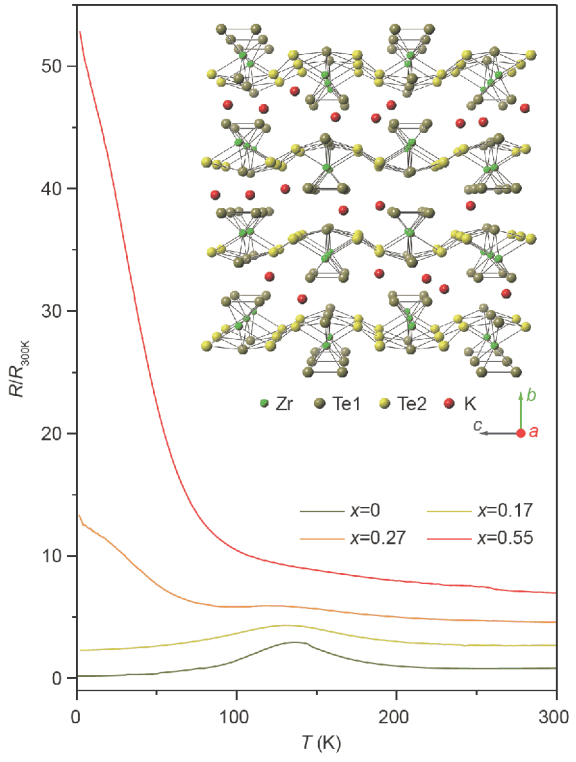


Figure 1 (Color online) Resistance (*R*) as measured on K-intercalated K_xZrTe_5 as a function of the temperature. *R* was normalized against its value at 300 K. The curves are shifted by 2 in the vertical direction for clarity. The inset shows the crystal structure of the single $ZrTe_5$ crystal having intercalated K atoms.

Figure 1 shows the temperature (T) dependence of the normalized resistance (R) as measured on different K_xZrTe_5 (x=0 to ~0.55) samples under a zero magnetic field. The current was applied along a-axis. For the pristine single $ZrTe_5$ single crystal, the R-T curve exhibits an anomalous resistance peak at around T_p≈135 K, and a typical metallic behavior at temperatures below T_p, which is in agreement with previous studies [45]. Surprisingly, the resistance at low temperatures increases tremendously upon intercalation of K atoms. At low temperatures, when x is greater than ~0.27, the sample undergoes a semimetal-to-semiconductor transition. Meanwhile, the anomalous resistance peak remained at ~135 K, although its intensity gradually decreased until disappearing when x is greater than ~0.55.

To further investigate the effect of the magnetic field on transport properties, we performed magnetoresistance measurements under magnetic fields of up to 5 T applied along the b-axis. Figure 2(a) and (b) show the magnetic field dependence of the longitudinal magnetoresistance (MR=[$R(H)$/$R(0)$−1]×100%) and the Hall resistance (R_{xy}), respectively, as measured on $K_{0.55}ZrTe_5$ samples at various temperatures. Due to the asymmetrical issue of the electrodes during the measurements, the MR and $R_{xy}(H)$ results were symmetrized. A positive MR effect was observed in all the explored temperature range (from 2 to 160 K) and the magnetic field range (from 0 to 5 T). It can be seen that $MR(H)$ roughly follows a $R \sim \sqrt{B}$ dependence at low temperatures, indicating the existence of a weak antilocalization effect [49]. Furthermore, as shown in Figure 2(a), the temperature dependence of the MR exhibits a similar trend as the intrinsic $ZrTe_5$, particularly the CVT-grown sample [44]: MR drops first and then increases as temperature increases. It is worth noting that for $K_{0.55}ZrTe_5$ the resistance peak was completely suppressed, as indicated in the R-T plot (Figure 1). Although

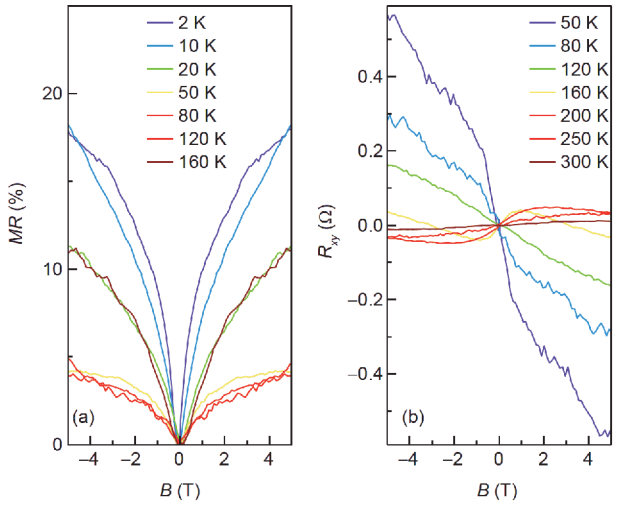


Figure 2 (Color online) Magnetic field dependence of (a) the longitudinal magnetoresistance (MR=[$R(H)$/$R(0)$−1]×100%) and (b) the Hall resistance (R_{xy}) as measured on $K_{0.55}ZrTe_5$ samples at various temperatures.

K_xZrTe_5 exhibited a similar behavior, the positive MR effect was significantly weaker by approximately one and a half orders of magnitude. For instance, previous studies showed a MR of ~900% at 5 T for CVT-grown $ZrTe_5$ [44], while that of $K_{0.55}ZrTe_5$ was only ~17%. Therefore, it was suggested that for $K_{0.55}ZrTe_5$ the influence of the magnetic field on resistance was small, but not negligible.

As shown in Figure 2(b), the Hall resistance (R_{xy}) exhibits a negative slope at low temperatures (T≤120-160 K), indicating that charge transport occurs primarily via electron carriers. As temperature increased to ~160 K, the Hall resistance at near zero magnetic field exhibits a sign reversal, consistent with the observations made for pristine $ZrTe_5$. Conversely, the positive slope of $R_{xy}(H)$ at T≥200 K demonstrates that charge transport occurs primarily via hole carriers. Even though the initial resistance peak is completely suppressed, for $K_{0.55}ZrTe_5$ the sign reversal still occurs near the region where this peak was (T_p~135 K). We believe that a temperature-induced Lifshitz transition [26], with a similar mechanism, can explain these phenomena.

To quantitatively understand the transport properties, the Hall conductivity, $\sigma_{xy} = \rho_{xy} / \left(\rho_{xx}{}^2+\rho_{xy}{}^2\right)$, was extracted and fitted with the two-carrier model [42],

$$\sigma_{xy} = eB\left(\pm\frac{n_1\mu_1^2}{1+\mu_1^2B^2} \pm \frac{n_2\mu_2^2}{1+\mu_2^2B^2}\right),$$

where $n_{1,2}$ and $\mu_{1,2}$ are the carrier density and the carrier mobility, respectively, and the plus (minus) sign represents the hole (electron) carriers. Figure 3(a) and (b) show the results obtained for $K_{0.55}ZrTe_5$: charge transport occurs via electron carriers at T<~160 K, and hole carriers start to emerge at T≈160 K; thus, at higher temperatures, hole carriers dominate while electron carriers disappear. There are two kinds of electron carriers at T<~160 K. At T≈20 K, the electron carrier density (n) for electron carriers 1 (e1) and 2 (e2) is 1.40×10^{17} and 2.37×10^{19} m^{-3}, respectively, and the mobility (μ) for e1 and e2 is 2.28 and 0.11 $m^2\ V^{-1}\ s^{-1}$, respectively. For reference, in pristine $ZrTe_5$ the electron carrier density is about five orders of magnitude lower, while the mobility remains largely the same, consistent with the semiconducting behavior observed in the R-T measurements. Conversely, the hole carrier mobility is greater than the electron carrier mobility, but the hole carrier density is lower, illustrated by an initial positive slope in $\rho_{xy}(H)$ followed by a sign reversal, which is consistent with the results obtained in previous studies [44]. Interestingly, it was observed that the temperature dependence of the hole carrier mobility is similar to that observed for flux-grown $ZrTe_5$ [44]. The carrier type reversal with temperature increase suggests the occurrence of a Lifshitz transition. In addition to the electron-hole competition, the carrier mobility and density may also play a role in the formation of the resistance peak, as proposed in a previous study on $ZrTe_5$ nanosheets [42].

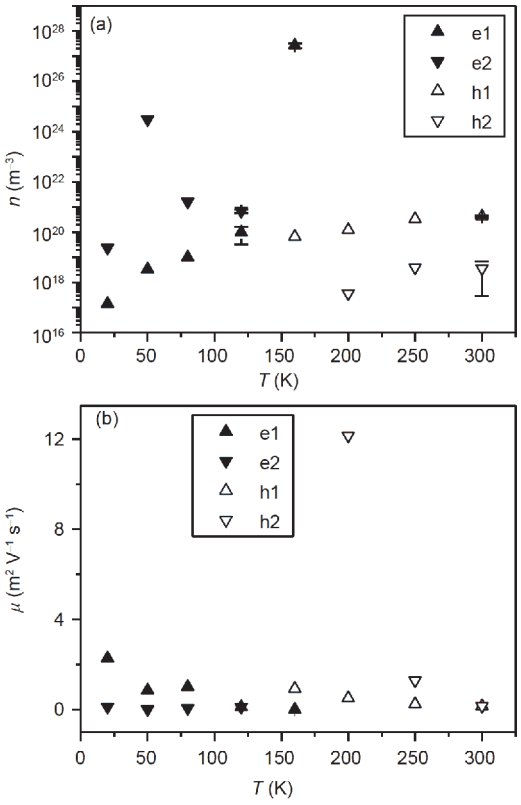


Figure 3 Temperature dependence of the carrier density (a) and the carrier mobility (b) for $K_{0.55}ZrTe_5$ as extracted from the fitting of the Hall conductivity data to the two-carrier model.

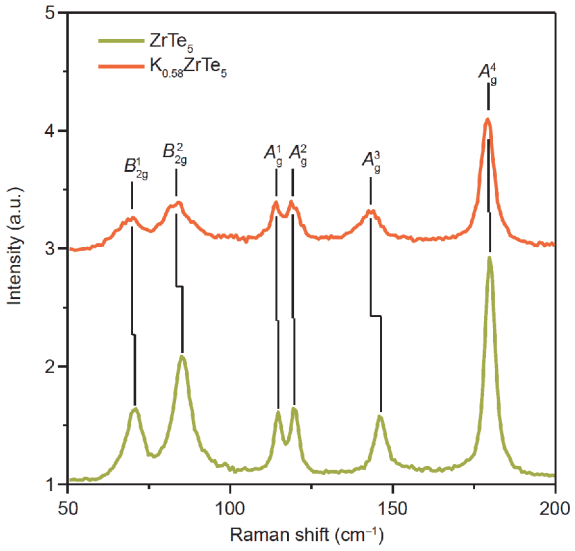


Figure 4 (Color online) Raman spectra of the single $ZrTe_5$ crystal before and after intercalation with K (x≈0.58) atoms. The peaks are marked with vertical lines to show the shift more clearly.

As previously reported [44], flux-grown single $ZrTe_5$ crystals also exhibit a semiconductor-like behavior, which was ascribed to the decrease in the number of Te vacancies. However, for K-intercalated $ZrTe_5$, a different mechanism should be considered because: 1) the location of the resistance peak does not change, but the intensity is greatly suppressed, and 2) the carrier type transition is still observed from 120 to 160 K. If taking into account only the electron-doping effect, the Fermi level should move upwards and thus, the opposite phenomenon would be observed, i.e., the sample should exhibit a more metallic behavior at low temperatures and the resistance peak would appear at higher temperatures. This suggests that the role of the electron-doping effect in K-intercalated $ZrTe_5$ may be negligible.

To further characterize the structural changes upon K intercalation, Raman spectroscopy measurements were performed for $ZrTe_5$ before and after intercalation of K atoms (Figure 4). According to previous studies [50-52], two B_{2g} modes and four A_g modes can be excited in the range between 50 and 200 cm^{-1} when a laser vertically irradiates the *ac*-plane. Accordingly, as shown in Figure 4, the characteristic peaks at 71.0 and 85.1 cm^{-1} can be assigned to the B_{2g} modes, while the other four peaks, at 114.8, 119.4, 145.8, and 179.8 cm^{-1}, are ascribed to the A_g modes. Upon K intercalation, the A_g^3 mode, at 145.8 cm^{-1}, shows a clear red shift to 143.3 cm^{-1}, while the A_g^4 mode, at 179.8 cm^{-1}, is nearly unchanged. Such spectral shift clearly suggests that the lattice constants change upon intercalation of K atoms. According to a previous study [40], the application of high pressure resulted in a reduced interlayer space and induced a blue shift in the Raman peak at 145.8 cm^{-1}. Conversely, it is reasonable to expect that the red shift of the Raman peak, observed for $K_{0.58}ZrTe_5$, is induced by an enlarged interlayer space and weakened interlayer coupling. Therefore, atom intercalation applies a sort of "tensile pressure", enlarging the lattice constant along the *b*-axis. A similar lattice expansion induced by atom intercalation has been reported for other layered materials [53,54]. However, in a recent study on K-intercalated WTe_2 [47] no lattice expansion could be detected. Why intercalation induces lattice expansion in some materials but not in others is a question that remains to be answered and requires further investigation.

Based on the above mentioned results and analyses, a reasonable mechanism that explains the observed phenomena was formulated (Figure 5). The pristine single $ZrTe_5$ crystal grown by CVT method is an n-type semiconductor, which exhibits metallic behavior at low temperatures, and the abnormal resistance peak is caused by a temperature-induced Lifshitz transition, as illustrated in Figure 5(a). The intercalation of K atoms into $ZrTe_5$ applies an effective "negative pressure" and induces a lattice expansion, especially along the *b*-axis. Assuming that pristine $ZrTe_5$ is a Dirac semimetal or a weak TI, such lattice expansion will definitely result in the enlargement of band gap. As a result, due to the antagonizing effects of lattice expansion and electron doping, the Fermi level shifts to the band gap region, as shown in Figure 5(b), resulting in an insulating behavior at

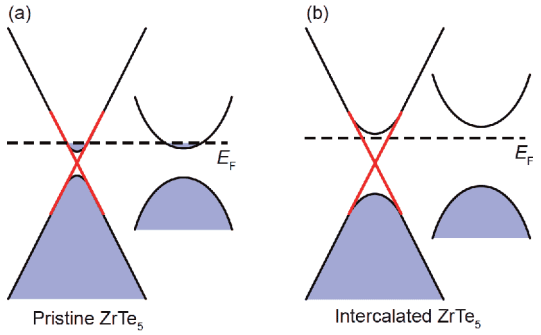


Figure 5 (Color online) Schematic illustration of the band structure of pristine $ZrTe_5$ (a) and atom-intercalated K_xZrTe_5 (b). The red lines represent the topological edge states. For pristine $ZrTe_5$, Fermi level crosses the conduction band at low temperature due to natural n-type doping. After atom intercalation, the band gap widens and therefore, the Fermi level is located within the band gap region.

low temperatures.

4 Conclusion

In summary, K atoms were intercalated into a single $ZrTe_5$ crystal by the liquid ammonia method, inducing a lattice expansion which led to the enlargement of band gap. As a result, a semimetal-to-semiconductor transition was induced in $ZrTe_5$ at a low temperature. In addition, the Hall sign reversal indicates the occurrence of a Lifshitz transition. A positive magnetoresistance effect exhibiting a $R \sim \sqrt{B}$ dependence at low temperatures was observed, which can be attributed to a weak antilocalization effect. This work provides an ideal platform to produce insulating $ZrTe_5$ for further research, particularly in relation to the transport properties of topological edge states.

This work was supported by the Ministry of Science and Technology of China (Grant Nos. 2014CB921103, and 2015CB921203), and the National Natural Science Foundation of China (Grant Nos. 11774149, 11790311, 11674157, 11674154, 51032003, 1171101156, 11374149, and 11374140).

1 S. Okada, T. Sambongi, and M. Ido, J. Phys. Soc. Jpn. **49**, 839 (1980).
2 T. E. Jones, W. W. Fuller, T. J. Wieting, and F. Levy, Solid State Commun. **42**, 793 (1982).
3 G. N. Kamm, D. J. Gillespie, A. C. Ehrlich, T. J. Wieting, and F. Levy, Phys. Rev. B **31**, 7617 (1985).
4 M. Izumi, T. Nakayama, K. Uchinokura, S. Harada, R. Yoshizaki, and E. Matsuura, J. Phys. C-Solid State Phys. **20**, 3691 (1987).
5 E. P. Stillwell, A. C. Ehrlich, G. N. Kamm, and D. J. Gillespie, Phys. Rev. B **39**, 1626 (1989).
6 R. T. Littleton IV, T. M. Tritt, J. W. Kolis, and D. R. Ketchum, Phys. Rev. B **60**, 13453 (1999).
7 M. Rubinstein, Phys. Rev. B **60**, 1627 (1999).
8 T. M. Tritt, N. D. Lowhorn, R. T. Littleton IV, A. Pope, C. R. Feger, and J. W. Kolis, Phys. Rev. B **60**, 7816 (1999).
9 H. Weng, X. Dai, and Z. Fang, Phys. Rev. X **4**, 011002 (2014), arXiv: 1309.7529.
10 Z. Fan, Q. F. Liang, Y. B. Chen, S. H. Yao, and J. Zhou, Sci. Rep. **7**, 45667 (2017), arXiv: 1611.04263.
11 J. Mutch, W. C. Chen, P. Went, T. Qian, I. Z. Wilson, A. Andreev, C. C. Chen, and J. H. Chu,. arXiv: 1808.07898
12 R. Y. Chen, Z. G. Chen, X. Y. Song, J. A. Schneeloch, G. D. Gu, F. Wang, and N. L. Wang, Phys. Rev. Lett. **115**, 176404 (2015), arXiv: 1506.08676.
13 R. Y. Chen, S. J. Zhang, J. A. Schneeloch, C. Zhang, Q. Li, G. D. Gu, and N. L. Wang, Phys. Rev. B **92**, 075107 (2015), arXiv: 1505.00307.
14 X. B. Li, W. K. Huang, Y. Y. Lv, K. W. Zhang, C. L. Yang, B. B. Zhang, Y. B. Chen, S. H. Yao, J. Zhou, M. H. Lu, L. Sheng, S. C. Li, J. F. Jia, Q. K. Xue, Y. F. Chen, and D. Y. Xing, Phys. Rev. Lett. **116**, 176803 (2016).
15 R. Wu, J. Z. Ma, S. M. Nie, L. X. Zhao, X. Huang, J. X. Yin, B. B. Fu, P. Richard, G. F. Chen, Z. Fang, X. Dai, H. M. Weng, T. Qian, H. Ding, and S. H. Pan, Phys. Rev. X **6**, 021017 (2016).
16 Q. Li, D. E. Kharzeev, C. Zhang, Y. Huang, I. Pletikosić, A. V. Fedorov, R. D. Zhong, J. A. Schneeloch, G. D. Gu, and T. Valla, Nat. Phys. **12**, 550 (2016), arXiv: 1412.6543.
17 X. Yuan, C. Zhang, Y. Liu, A. Narayan, C. Song, S. Shen, X. Sui, J. Xu, H. Yu, Z. An, J. Zhao, S. Sanvito, H. Yan, and F. Xiu, NPG Asia Mater. **8**, e325 (2016).
18 G. Zheng, J. Lu, X. Zhu, W. Ning, Y. Han, H. Zhang, J. Zhang, C. Xi, J. Yang, H. Du, K. Yang, Y. Zhang, and M. Tian, Phys. Rev. B **93**, 115414 (2016), arXiv: 1603.05351.
19 W. Yu, Y. Jiang, J. Yang, Z. L. Dun, H. D. Zhou, Z. Jiang, P. Lu, and W. Pan, Sci. Rep. **6**, 35357 (2016), arXiv: 1602.06824.
20 Y. Liu, X. Yuan, C. Zhang, Z. Jin, A. Narayan, C. Luo, Z. Chen, L. Yang, J. Zou, X. Wu, S. Sanvito, Z. Xia, L. Li, Z. Wang, and F. Xiu, Nat. Commun. **7**, 12516 (2016).
21 G. Manzoni, L. Gragnaniello, G. Autès, T. Kuhn, A. Sterzi, F. Cilento, M. Zacchigna, V. Enenkel, I. Vobornik, L. Barba, F. Bisti, P. Bugnon, A. Magrez, V. N. Strocov, H. Berger, O. V. Yazyev, M. Fonin, F. Parmigiani, and A. Crepaldi, Phys. Rev. Lett. **117**, 237601 (2016), arXiv: 1608.03433.
22 L. Moreschini, J. C. Johannsen, H. Berger, J. Denlinger, C. Jozwiack, E. Rotenberg, K. S. Kim, A. Bostwick, and M. Grioni, Phys. Rev. B **94**, 081101 (2016).
23 Z. G. Chen, R. Y. Chen, R. D. Zhong, J. Schneeloch, C. Zhang, Y. Huang, F. Qu, R. Yu, Q. Li, G. D. Gu, and N. L. Wang, Proc. Natl. Acad. Sci. **114**, 816 (2017), arXiv: 1701.07726.
24 Y. X. Wang, Eur. Phys. J. B **90**, 99 (2017).
25 Y. Jiang, Z. L. Dun, H. D. Zhou, Z. Lu, K. W. Chen, S. Moon, T. Besara, T. M. Siegrist, R. E. Baumbach, D. Smirnov, and Z. Jiang, Phys. Rev. B **96**, 041101 (2017), arXiv: 1703.08193.
26 Y. Zhang, C. Wang, L. Yu, G. Liu, A. Liang, J. Huang, S. Nie, X. Sun, Y. Zhang, B. Shen, J. Liu, H. Weng, L. Zhao, G. Chen, X. Jia, C. Hu, Y. Ding, W. Zhao, Q. Gao, C. Li, S. He, L. Zhao, F. Zhang, S. Zhang, F. Yang, Z. Wang, Q. Peng, X. Dai, Z. Fang, Z. Xu, C. Chen, and X. J. Zhou, Nat. Commun. **8**, 15512 (2017), arXiv: 1602.03576.
27 G. Manzoni, A. Crepaldi, G. Autès, A. Sterzi, F. Cilento, A. Akrap, I. Vobornik, L. Gragnaniello, P. Bugnon, M. Fonin, H. Berger, M. Zacchigna, O. V. Yazyev, and F. Parmigiani, J. Electron Spectr. Related Phenom. **219**, 9 (2017).
28 L. Shen, M. X. Wang, S. C. Sun, J. Jiang, X. Xu, T. Zhang, Q. H. Zhang, Y. Y. Lv, S. H. Yao, Y. B. Chen, M. H. Lu, Y. F. Chen, C. Felser, B. H. Yan, Z. K. Liu, L. X. Yang, and Y. L. Chen, J. Electron Spectr. Related Phenom. **219**, 45 (2017).
29 H. Xiong, J. A. Sobota, S. L. Yang, H. Soifer, A. Gauthier, M. H. Lu, Y. Y. Lv, S. H. Yao, D. Lu, M. Hashimoto, P. S. Kirchmann, Y. F. Chen, and Z. X. Shen, Phys. Rev. B **95**, 195119 (2017), arXiv: 1704.05161.
30 Y. Y. Lv, B. B. Zhang, X. Li, K. W. Zhang, X. B. Li, S. H. Yao, Y. B. Chen, J. Zhou, S. T. Zhang, M. H. Lu, S. C. Li, and Y. F. Chen, Phys. Rev. B **97**, 115137 (2018).
31 N. L. Nair, P. T. Dumitrescu, S. Channa, S. M. Griffin, J. B. Neaton, A. C. Potter, and J. G. Analytis, Phys. Rev. B **97**, 041111 (2018).
32 W. Wang, X. Zhang, H. Xu, Y. Zhao, W. Zou, L. He, and Y. Xu, Sci.

Rep. **8**, 5125 (2018).
33 G. Zheng, X. Zhu, Y. Liu, J. Lu, W. Ning, H. Zhang, W. Gao, Y. Han, J. Yang, H. Du, K. Yang, Y. Zhang, and M. Tian, Phys. Rev. B **96**, 121401 (2017), arXiv: 1607.05384.
34 J. Wang, J. Niu, B. Yan, X. Li, R. Bi, Y. Yao, D. Yu, and X. Wu, Proc. Natl. Acad. Sci. **115**, 9145 (2018).
35 F. D. Tang, Y. R. Ren, P. P. Wang, R. D. Zhong, J. Schneeloch, S. A. Yang, K. Yang, P. A. Lee, G. Gu, Z. Qiao, L. Zhang,. arXiv: 1807.02678
36 T. Liang, J. Lin, Q. Gibson, S. Kushwaha, M. Liu, W. Wang, H. Xiong, J. A. Sobota, M. Hashimoto, P. S. Kirchmann, Z. X. Shen, R. J. Cava, and N. P. Ong, Nat. Phys. **14**, 451 (2018).
37 P. Li, C. H. Zhang, J. W. Zhang, Y. Wen, and X. X. Zhang, Phys. Rev. B **98**, 121108 (2018), arXiv: 1803.01213.
38 H. Wang, H. Liu, Y. Li, Y. Liu, J. Wang, J. Liu, J. Y. Dai, Y. Wang, L. Li, J. Yan, D. Mandrus, X. C. Xie, and J. Wang, Sci. Adv. **4**, eaau5096 (2018), arXiv: 1704.00995.
39 H. W. Liu, H. Jiang, Z. Q. Wang, R. Joynt, and X. C. Xie,. arXiv: 1807.02459
40 Y. Zhou, J. Wu, W. Ning, N. Li, Y. Du, X. Chen, R. Zhang, Z. Chi, X. Wang, X. Zhu, P. Lu, C. Ji, X. Wan, Z. Yang, J. Sun, W. Yang, M. Tian, Y. Zhang, and H. K. Mao, Proc. Natl. Acad. Sci. **113**, 2904 (2016), arXiv: 1505.02658.
41 J. L. Zhang, C. Y. Guo, X. D. Zhu, L. Ma, G. L. Zheng, Y. Q. Wang, L. Pi, Y. Chen, H. Q. Yuan, and M. L. Tian, Phys. Rev. Lett. **118**, 206601 (2017), arXiv: 1701.03283.
42 J. Lu, G. Zheng, X. Zhu, W. Ning, H. Zhang, J. Yang, H. Du, K. Yang, H. Lu, Y. Zhang, and M. Tian, Phys. Rev. B **95**, 125135 (2017), arXiv: 1611.08679.
43 J. Niu, J. Wang, Z. He, C. Zhang, X. Li, T. Cai, X. Ma, S. Jia, D. Yu, and X. Wu, Phys. Rev. B **95**, 035420 (2017), arXiv: 1511.09315.
44 P. Shahi, D. J. Singh, J. P. Sun, L. X. Zhao, G. F. Chen, Y. Y. Lv, J. Li, J. Q. Yan, D. G. Mandrus, and J. G. Cheng, Phys. Rev. X **8**, 021055 (2018).
45 Y. Y. Lv, F. Zhang, B. B. Zhang, B. Pang, S. H. Yao, Y. B. Chen, L. Ye, J. Zhou, S. T. Zhang, and Y. F. Chen, J. Cryst. Growth **457**, 250 (2017).
46 T. Ying, X. Chen, G. Wang, S. Jin, X. Lai, T. Zhou, H. Zhang, S. Shen, and W. Wang, J. Am. Chem. Soc. **135**, 2951 (2013).
47 L. Zhu, Q. Y. Li, Y. Y. Lv, S. Li, X. Y. Zhu, Z. Y. Jia, Y. B. Chen, J. Wen, and S. C. Li, Nano Lett. **18**, 6585 (2018).
48 H. Fjellvåg, and A. Kjekshus, Solid State Commun. **60**, 91 (1986).
49 H. Z. Lu, and S. Q. Shen, Phys. Rev. B **92**, 035203 (2015), arXiv: 1411.2686.
50 G. Qiu, Y. Du, A. Charnas, H. Zhou, S. Jin, Z. Luo, D. Y. Zemlyanov, X. Xu, G. J. Cheng, and P. D. Ye, Nano Lett. **16**, 7364 (2016), arXiv: 1606.07960.
51 I. Taguchi, A. Grisel, and F. Levy, Solid State Commun. **46**, 299 (1983).
52 A. Zwick, G. Landa, R. Carles, M. A. Renucci, and A. Kjekshus, Solid State Commun. **44**, 89 (1982).
53 R. B. Somoano, V. Hadek, and A. Rembaum, J. Chem. Phys. **58**, 697 (1973).
54 M. Fujioka, C. Wu, N. Kubo, G. Zhao, A. Inoishi, S. Okada, S. Demura, H. Sakata, M. Ishimaru, H. Kaiju, and J. Nishii, J. Am. Chem. Soc. **139**, 17987 (2017).